Interplanetary Optical Navigation

V. Hunter Adams* and Mason Peck †
Cornell University, Ithaca NY, 14853

This paper describes a general approach to optical navigation based on sightings of moons, planets, and the sun for spacecraft without access to Earth-based ranging resources. This analysis addresses the particular case of the Earth-Sun-Moon system. Using this approach, a spacecraft can autonomously determine its position relative in Earth-Centered Inertial (ECI) coordinate frame. It does so by performing a Gauss-Newton optimization on measurements of the angular width and the angular separation of the Earth, Sun, and Moon. In nonsingular configurations of the celestial bodies, this method is capable of determining position to within tens of kilometers without modeling any attitude dynamics and assuming the imaging performance of an inexpensive Raspberry Pi camera module. The method for navigation described in this paper can be applied to any appropriately equipped spacecraft operating in regions of space with analogous celestial objects.

I. Introduction

The rapid improvement of commercial-off-the-shelf (COTS) hardware has made missions to low-Earth-orbit (LEO) and near-Earth space possible at a fraction of the cost of traditional spacecraft. This trend is especially apparent in the CubeSat community, where universities, entrepreneurs, and hobbyists have created flight-ready spacecraft for less than $10,000 and have used them to perform scientifically and commercially relevant missions[10]. The relevance of CubeSats for scientific and commercial purposes in LEO continues to grow. San Francisco's Planet Labs deployed 28 CubeSats in their Flock-1 constellation last year, which now provide commercially valuable imagery to agricultural, civil government, geospatial, and natural resources industries.[7] In the year prior, 80 CubeSats were launched, only 5 of which were commercial. Over half came from universities, with civil and military missions making up the remainder of the manifests. These numbers have continued to grow in the last two years[10].

The success of CubeSats in LEO is a compelling argument for conducting similar missions in deep space. Interplanetary missions offer an opportunity to collect commercially and scientifically valuable data that is impossible for LEO spacecraft (such as asteroid/comet information for those interested in studying, visiting, or mining those objects), and to test technologies that require the unique environment that deep space offers. Unfortunately, with increased distance comes more expensive and more specialized equipment for navigating and communicating with spacecraft[8]. This cost begins to defeat the purpose of a cheap, COTS-based architecture and has prevented many companies and universities from using CubeSats beyond LEO.

It is partially for this reason that NASA identified deep-space communication technology as a technology gap in the 2014 Small Spacecraft Technology State of the Art report[9]. There is strong motivation to create navigation systems that allow CubeSats to determine their locations for themselves, without the aid of Earth-based systems that require two-way data transmission, the power for which is difficult to generate on a small spacecraft. Autonomous navigation technology would remove one of the greatest barriers to entry for deep-space CubeSat missions by reducing the costs of navigation. A system like this would help enable the type of science, research, and commercial development occurring in LEO to take place in deep space.

What follows describes one means of accomplishing this goal in regions of space containing planets, moons, and other objects that are significantly brighter than background stars. We consider a specific example of cislunar navigation: by using onboard COTS cameras to take photographs of the Earth, Sun,

*Graduate Research Assistant, Sibley School of Mechanical and Aerospace Engineering, 127 Upson Hall, Ithaca NY 14853, AIAA Student Member
†Associate Professor, Sibley School of Mechanical and Aerospace Engineering, 212 Upson Hall, Ithaca NY 14853, AIAA Full Member

and Moon, a spacecraft can determine its location without the aid of Earth-based systems, without explicit attitude determination, and without an accurate attitude-dynamics model. This analysis treats a particular trans-lunar injection trajectory with additive noise from unmodeled or mismodeled gravitational effects, external forces, and thruster pulses. This trajectory represents a general trajectory extremely well since it contains quickly changing dynamics during lunar flybys, periods during which the celestial bodies assume singular configurations, and periods during which the celestial bodies are nonsingular. It also demonstrates the navigation method's performance in extremely close proximity to celestial bodies and at more distant locations.

Some of the measurement techniques employed in this paper have been studied by John Christian and by members of the robotics community. Christian's research on Centroid and Apparent Diameter Optical Navigation (CAD OPNAV) provides valuable insight to the image processing that is required to employ the method of navigation described in this paper. In [2], Christian *et al.* estimate distance to the Moon using its apparent diameter in various illumination conditions. They do so by performing edge extraction on gathered image data, and then fitting an ellipse to the extracted edge. Using this technique, Christian has demonstrated estimating distance to the moon to within 762.7 km using a photograph taken from Earth[3]. In [3] and [4], Christian develops an algorithm for extracting navigation information from photographs on orbit, and uses that algorithm to construct an Extended Kalman Filter for image data from the MESSENGER fly-by of Venus. These provide insight into the image processing that is required to gather the information that the method of navigation described in this paper takes as inputs.

In the robotics community, similar techniques are used for visual navigation and pose estimation. In visual navigation, data from images of the environment pass through a Kalman filter to estimate the location and velocity of nearby obstacles[1]. The robot then uses this information to alter its trajectory in response to its environment. Similarly, in pose estimation, a robot attempts to estimate its position in an unknown environment where it has no frame of reference except the features that it gathers from images of its surroundings. Lu and Milos solve this problem by taking two scans of the environment and performing a point-to-point least squares to find displacement between scans[5]. Both of these problems are closely related to that of determining position relative to nearby planets, moons, and the sun.

What follows departs from existing work in that navigation is performed without modeling any spacecraft attitude or position dynamics; the position is calculated relative to a geometry established by the ephemerides of the celestial bodies. One advantage of this approach is that it obviates the need for a star tracker or related hardware (and algorithms), enabling the technique to operate in a stand-alone fashion or on a fast-spinning spacecraft. This paper takes a different approach from the work of Christian. It does not attempt to fit an ellipse to a single body with high precision but, instead, includes multiple celestial bodies, enabling three degree-of-freedom navigation in the vicinity of these objects. It departs from existing pose estimation work in that the reference objects (celestial bodies) change their position with time, leading to singularities that are not present in many robotics applications.

II. Articulating the Problem

The spacecraft in question has onboard cameras that provide digital images of the Earth, Sun, and Moon. An on-board ephemeris for each of these objects is assumed to provide perfect knowledge of the vectors relating the Earth, Sun, and Moon; an on-board real-time clock (infrequently updated from the ground) provides arbitrarily accurate time knowledge. The cameras provide noisy measurements of the vectors from the spacecraft to each celestial body. This information falls into two broad categories: information independent of any coordinate system and information expressed in a particular coordinate system. Information independent of any coordinate system includes the magnitudes of the distances among objects and the angles among the vectors between objects. Particular to the ECI and spacecraft body coordinate systems are the parametrizations of the vectors from each celestial body to every other celestial body and the parametrizations of the vectors from the spacecraft to each celestial body, respectively. Navigation requires the parametrization, in a useful coordinate system, of the vector from Earth to spacecraft. By exploiting the time-varying but known geometry of the Earth, Sun, Moon system; one can decouple the position determination problem from the attitude determination problem without losing any information about location. This is the problem that is treated in this paper. This paper considers a Gauss-Newton method for position determination, which uses instantaneous measurements alone to obtain an instantaneous position estimate. The performance of the Gauss-Newton method is baselined against that of an Extended Kalman Filter,

which uses both measurements and dynamics to obtain estimates for spacecraft position and velocity.

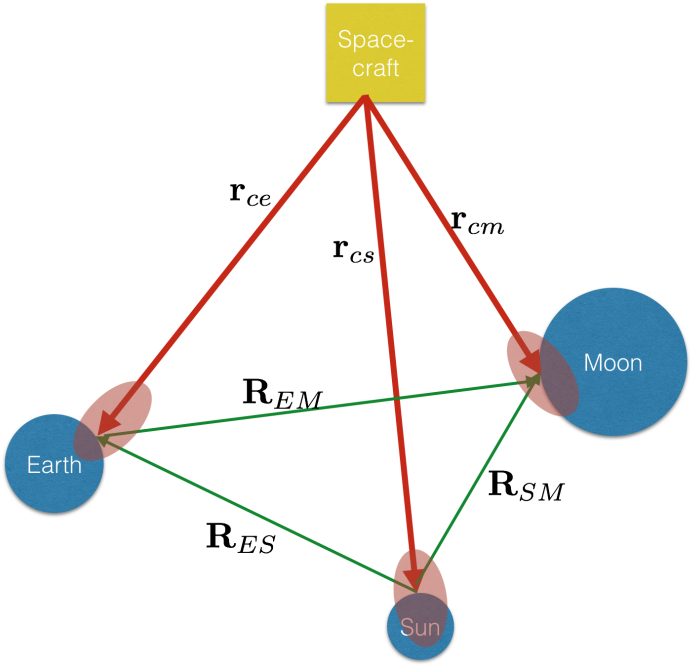

Figure 1: Illustration of the geometry of the system. The thin, green vectors are represented in ECI and are known with absolute certainty. The thick, red vectors are represented in Body coordinates with noise represented by the ellipses.

III. True and Nominal Trajectories

The trans-lunar trajectory shown in Figure 2 is considered as a case study in this analysis. The nominal trajectory is plotted alongside the true trajectory, which includes additive noise in the form of unmodeled white stochastic accelerations. These unmodeled accelerations lead to a random walk in the spacecraft position of up to 10,000 km from the nominal trajectory. The effect of acceleration noise on position can be determined by representing the dynamics in the state-space representation in eq. (1), which shows the relationship between a particular position coordinate, x_i, and its first two derivatives. Eq. (2) shows the state-transition matrix for the system, formed by taking the matrix exponential of the dynamics matrix in eq. (1).

$$\begin{bmatrix} \dot{x_i} \\ \ddot{x_i} \\ \dddot{x_i} \end{bmatrix} = \begin{bmatrix} 0 & 1 & 0 \\ 0 & 0 & 1 \\ 0 & 0 & 0 \end{bmatrix} \begin{bmatrix} x_i \\ \dot{x_i} \\ \ddot{x_i} \end{bmatrix} \tag{1}$$

$$\Phi(t, t_0) = \begin{bmatrix} 1 & \Delta t & \frac{\Delta t^2}{2} \\ 0 & 1 & \Delta t \\ 0 & 0 & 1 \end{bmatrix} \tag{2}$$

The relationship between acceleration input and the position/velocity state variables are given by the top two components of the third column of the state-transition matrix shown in eq. (2). Rewriting the system model with stochastic acceleration disturbances included leads to the state-update equation shown in eq. (3).

$$\mathbf{x}_{i,k} = \begin{bmatrix} 1 & \Delta t \\ 0 & 1 \end{bmatrix} \mathbf{x}_{i,k-1} + \begin{bmatrix} a_{i,k}\frac{\Delta t^2}{2} \\ a_{i,k}\Delta t \end{bmatrix} \tag{3}$$

Taking the covariance of the additive noise, and expanding to include all three position coordinates (x, y, and z in an ECI frame) leads to the process noise covariance shown in eq. (4).

$$Q = \begin{bmatrix} \frac{\Delta t^4}{4}\sigma_x^2 & 0 & 0 & \frac{\Delta t^3}{2}\sigma_x^2 & 0 & 0 \\ 0 & \frac{\Delta t^4}{4}\sigma_y^2 & 0 & 0 & \frac{\Delta t^3}{2}\sigma_y^2 & 0 \\ 0 & 0 & \frac{\Delta t^4}{4}\sigma_z^2 & 0 & 0 & \frac{\Delta t^3}{2}\sigma_z^2 \\ \frac{\Delta t^3}{2}\sigma_x^2 & 0 & 0 & \Delta t^2\sigma_x^2 & 0 & 0 \\ 0 & \frac{\Delta t^3}{2}\sigma_y^2 & 0 & 0 & \Delta t^2\sigma_y^2 & 0 \\ 0 & 0 & \frac{\Delta t^3}{2}\sigma_z^2 & 0 & 0 & \Delta t^2\sigma_z^2 \end{bmatrix} \tag{4}$$

where σ_x, σ_y, and σ_z in eq. (4) are the independent variances of the unmodeled zero-mean accelerations in the x, y, and z directions. Δt is the amount of time between position estimates (30 minutes in this analysis). The true trajectory is formed from the nominal trajectory by including this process noise. For purposes of this analysis, an acceleration variance of 5×10^{-10} km/s^2 has been assumed, leading to an unmodeled ΔV of 90 m/s every 30 minutes, assuming a 1σ additive acceleration. The true trajectory is the truth model for this analysis. In practice, much lower process noise would be expected, but unmodeled biases (not addressed in this paper), such as solar-radiation pressure force are important to assess. The use of a relatively high process noise is meant to illustrate the robustness of this technique in the presence of general unmodeled effects.

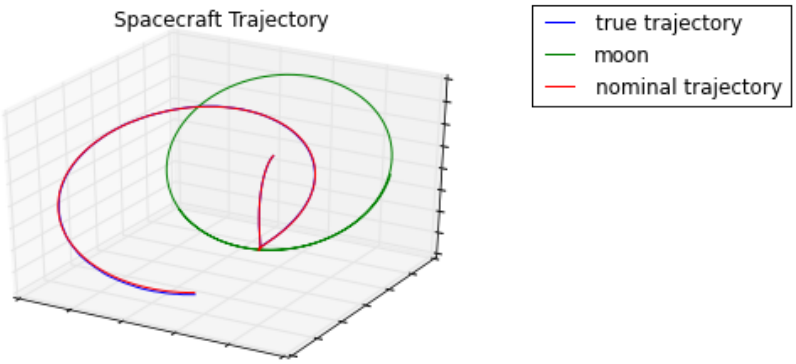

Figure 2: Spacecraft true and nominal trajectories

IV. The Gauss-Newton Measurement Model

IV.A. Constructing the Measurement Model

The vectors from the spacecraft to each celestial body can be represented as linear combinations of the vector from the spacecraft to the Earth and the vectors among Earth, Sun, and Moon. It is convenient to construct the problem in this way because the vectors among all celestial bodies are known from their respective ephemerides. In eqs. (5-7); d_{mx}, d_{my}, and d_{mz} represent the coordinates of the moon in an ECI coordinate frame (known quantities, assuming known time). Similarly, d_{sx}, d_{sy}, and d_{sz} represent the position of the Sun. The variables x, y, and z represent the coordinates of the Earth relative to the spacecraft in an ECI coordinate frame. These quantities must be obtained to solve the navigation problem.

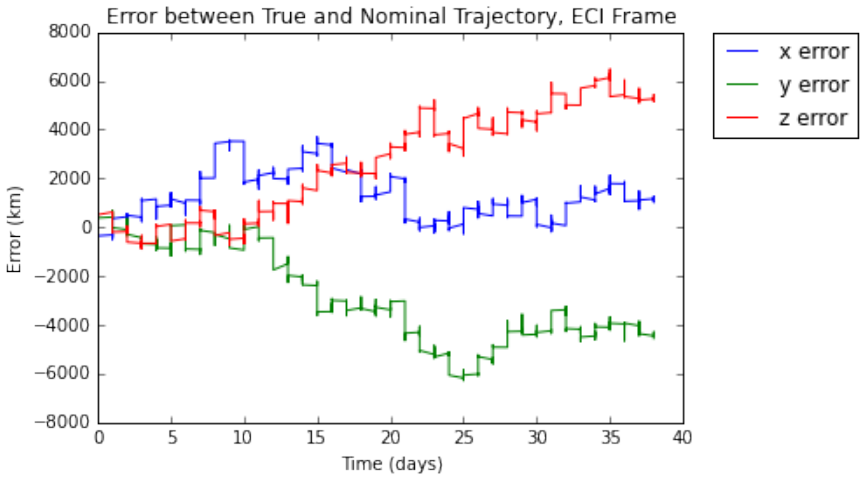

Figure 3: Accumulated position error between spacecraft true and nominal trajectories

$$^{E}r_{ce} = [x, y, z]^T \tag{5}$$

$$^{E}r_{cm} = [x + d_{mx}, y + d_{my}, z + d_{mz}]^T \tag{6}$$

$$^{E}r_{cs} = [x + d_{sx}, y + d_{sy}, z + d_{sz}]^T \tag{7}$$

From eqs. (5-7), it is possible to obtain the unit vectors from the spacecraft to each celestial body. Doing so is useful for constructing the nonlinear functions $h(\mathbf{x})$ that relate measurements to unknown state variables.

$$^{E}\hat{r}_{ce} = \begin{bmatrix} \frac{x}{(x^2+y^2+z^2)^{\frac{1}{2}}} \\ \frac{y}{(x^2+y^2+z^2)^{\frac{1}{2}}} \\ \frac{z}{(x^2+y^2+z^2)^{\frac{1}{2}}} \end{bmatrix} \tag{8}$$

$$^{E}\hat{r}_{cm} = \begin{bmatrix} \frac{x+d_{mx}}{((x+d_{mx})^2+(y+d_{my})^2+(z+d_{mz})^2)^{\frac{1}{2}}} \\ \frac{y+d_{my}}{((x+d_{mx})^2+(y+d_{my})^2+(z+d_{mz})^2)^{\frac{1}{2}}} \\ \frac{z+d_{mz}}{((x+d_{mx})^2+(y+d_{my})^2+(z+d_{mz})^2)^{\frac{1}{2}}} \end{bmatrix} \tag{9}$$

$$^{E}\hat{r}_{cs} = \begin{bmatrix} \frac{x+d_{sx}}{((x+d_{sx})^2+(y+d_{sy})^2+(z+d_{sz})^2)^{\frac{1}{2}}} \\ \frac{y+d_{sy}}{((x+d_{sx})^2+(y+d_{sy})^2+(z+d_{sz})^2)^{\frac{1}{2}}} \\ \frac{z+d_{sz}}{((x+d_{sx})^2+(y+d_{sy})^2+(z+d_{sz})^2)^{\frac{1}{2}}} \end{bmatrix} \tag{10}$$

From these vectors of unknown state variables and known quantities, it is possible to compute the quantities that the onboard cameras are capable of measuring directly. Among these quantities are the angular separations between each of the celestial bodies. The angular separation, measured in radians, is a number between 0 and π that represents the magnitude of the smaller angle separating two bodies. Since, in the range $[0, \pi]$, there is a one-to-one mapping between an angle and the cosine of that angle; this information can be represented as a cosine of the angle of separation without any loss of information. This cosine arises naturally from the vectors shown in eqs. (8-10). Constructing these measurements (the cosine of the angle of separation of each planet) by dotting the vectors of eqs. (8-10) yields eqs. (11-13).

$$\zeta_1 = \cos\theta_{ecm} = \left[\frac{x d_{\mathrm{mx}} + y d_{\mathrm{my}} + z d_{\mathrm{mz}} + x^2 + y^2 + z^2}{\sqrt{x^2+y^2+z^2}\sqrt{(d_{\mathrm{mx}}+x)^2 + (d_{\mathrm{my}}+y)^2 + (d_{\mathrm{mz}}+z)^2}} \right] \tag{11}$$

$$\zeta_2 = \cos\theta_{ecs} = \left[\frac{x d_{\mathrm{sx}} + y d_{\mathrm{sy}} + z d_{\mathrm{sz}} + x^2 + y^2 + z^2}{\sqrt{x^2+y^2+z^2}\sqrt{(d_{\mathrm{sx}}+x)^2 + (d_{\mathrm{sy}}+y)^2 + (d_{\mathrm{sz}}+z)^2}} \right] \tag{12}$$

$$\zeta_3 = \cos\theta_{mcs} = \left[\frac{d_{\mathrm{mx}}(d_{\mathrm{sx}}+x) + d_{\mathrm{my}}(d_{\mathrm{sy}}+y) + d_{\mathrm{sz}}(d_{\mathrm{mz}}+z) + z d_{\mathrm{mz}} + x d_{\mathrm{sx}} + y d_{\mathrm{sy}} + x^2 + y^2 + z^2}{\sqrt{(d_{\mathrm{mx}}+x)^2 + (d_{\mathrm{my}}+y)^2 + (d_{\mathrm{mz}}+z)^2}\sqrt{(d_{\mathrm{sx}}+x)^2 + (d_{\mathrm{sy}}+y)^2 + (d_{\mathrm{sz}}+z)^2}} \right] \tag{13}$$

where $\zeta_{1,2,3}$ are all constrained to $[-1, 1]$. It is tempting also to include sine measurements, but these are impossible to include without first solving the attitude determination problem. The cosine is agnostic to the sign of the angle, while the sine is not. Unless the attitude determination problem is solved first, the only available information is the magnitudes of the angles of separation.

The camera also provides data that yields the width of each celestial body in pixels, which simple to convert to a measurement of the angle subtended by that body. The mean radius of each celestial body is also a known quantity. Christian would also estimate the major and minor axes of an ellipse that fits this data, but the present algorithm does not take advantage of such information. d_e and d_m of eqs. (14-15) are the mean radii of the Earth and Moon, measured in kilometers. The measurement of the angular width of the Sun is omitted because, for any trajectory in cislunar space, it does not change appreciably enough to provide new information.

$$\zeta_4 = \theta_e = 2\tan^{-1}\left(\frac{d_e}{\sqrt{x^2+y^2+z^2}} \right) \tag{14}$$

$$\zeta_5 = \theta_m = 2\tan^{-1}\left(\frac{d_m}{\sqrt{(x+d_{mx})^2 + (y+d_{my})^2 + (z+d_{mz})^2}} \right) \tag{15}$$

Assembling these equations and the measured data yields the full set of nonlinear equations that relate camera measurements to unknown state variables. By convention, this set of nonlinear equations is $h(\mathbf{x})$.

$$\begin{bmatrix} \zeta_1 \\ \zeta_2 \\ \zeta_3 \\ \zeta_4 \\ \zeta_5 \end{bmatrix} = \begin{bmatrix} h_1(\mathbf{x}) \\ h_2(\mathbf{x}) \\ h_3(\mathbf{x}) \\ h_4(\mathbf{x}) \\ h_5(\mathbf{x}) \end{bmatrix} = h(\underline{\mathbf{x}}) \tag{16}$$

where each h_i is given by eqs. (11-15).

IV.B. Ambiguities and Singularities

Assuming that the celestial bodies are in a non-singular configuration (they span R^2), then these measurements isolate the spacecraft to one of two positions. One is above the plane formed by the Earth, Sun, and Moon, and the other is symmetrically below the plane. This symmetry becomes apparent when one transforms the vectors of eqs. (8-10) from the ECI coordinates to a coordinate system generated by performing a Gram-Schmidt orthogonalization of the vectors from Earth to Moon and Earth to Sun, defined by unit vectors $\hat{\mathbf{e}}_{\tilde{x}}$, $\hat{\mathbf{e}}_{\tilde{y}}$, and $\hat{\mathbf{e}}_{\tilde{z}}$. Doing so defines a coordinate system in which the $\hat{\mathbf{e}}_{\tilde{x}}$ axis points from the Earth to the Moon, the $\hat{\mathbf{e}}_{\tilde{y}}$ axis is orthogonal to the $\hat{\mathbf{e}}_{\tilde{x}}$ axis and points in the direction of the Sun, and the $\hat{\mathbf{e}}_{\tilde{z}}$ axis is orthogonal to the plane formed by the Earth, Sun, and Moon.

$$\hat{\mathbf{e}}_{\tilde{x}} = \frac{\mathbf{R}_{EM}}{||\mathbf{R}_{ES}||} \tag{17}$$

$$i = \hat{\mathbf{e}}_{\tilde{x}} \cdot \mathbf{R}_{ES} \tag{18}$$

$$\hat{\mathbf{e}}_{\tilde{y}} = \frac{\mathbf{R}_{ES} - i\hat{\mathbf{e}}_{\tilde{x}}}{||\mathbf{R}_{ES} - i\hat{\mathbf{e}}_{\tilde{x}}||} \tag{19}$$

$$\hat{\mathbf{e}}_{\tilde{z}} = \hat{\mathbf{e}}_{\tilde{x}} \times \hat{\mathbf{e}}_{\tilde{y}} \tag{20}$$

where $\mathbf{R}_{EM}$ is the vector connecting Earth to Moon and $\mathbf{R}_{ES}$ is the vector connecting Earth to Sun. The transformation from the ECI to these time-varying coordinates defined by the ephemerides (the "ephemeral" frame, denoted by superscript e) is formed by stacking these unit vectors into a rotation matrix. The transformation from the spacecraft body frame to the ephemeral frame can also be formed directly from measurements. This is not done in practice, but it is useful for studying the ambiguities and singularities in the measurement model.

$${}^{e}Q^{E} = \begin{bmatrix} {}^{E}\hat{e}_{\tilde{x}} & {}^{E}\hat{e}_{\tilde{y}} & {}^{E}\hat{e}_{\tilde{z}} \end{bmatrix} \tag{21}$$

$${}^{e}Q^{B} = \begin{bmatrix} {}^{B}\hat{e}_{\tilde{x}} & {}^{B}\hat{e}_{\tilde{y}} & {}^{B}\hat{e}_{\tilde{z}} \end{bmatrix} \tag{22}$$

By construction of the frame, the Earth, Sun, and Moon share the same $\tilde{z}$ coordinate and eqs. (8-10) can be transformed to the form shown in eq. (23).

$${}^{e}\hat{r}_{ce} = \begin{bmatrix} \frac{\tilde{x}}{(\tilde{x}^2+\tilde{y}^2+\tilde{z}^2)^{\frac{1}{2}}} \\ \frac{\tilde{y}}{(\tilde{x}^2+\tilde{y}^2+\tilde{z}^2)^{\frac{1}{2}}} \\ \frac{\tilde{z}}{(\tilde{x}^2+\tilde{y}^2+\tilde{z}^2)^{\frac{1}{2}}} \end{bmatrix} \quad {}^{e}\hat{r}_{cm} = \begin{bmatrix} \frac{\tilde{x}+\tilde{d}_{mx}}{\left((\tilde{x}+\tilde{d}_{mx})^2+\tilde{y}^2+\tilde{z}^2\right)^{\frac{1}{2}}} \\ \frac{\tilde{y}}{\left((\tilde{x}+\tilde{d}_{mx})^2+\tilde{y}^2+\tilde{z}^2\right)^{\frac{1}{2}}} \\ \frac{\tilde{z}}{\left((\tilde{x}+\tilde{d}_{mx})^2+\tilde{y}^2+\tilde{z}^2\right)^{\frac{1}{2}}} \end{bmatrix} \quad {}^{e}\hat{r}_{cs} = \begin{bmatrix} \frac{\tilde{x}+\tilde{d}_{sx}}{\left((\tilde{x}+\tilde{d}_{sx})^2+(\tilde{y}+\tilde{d}_{sy})^2+\tilde{z}^2\right)^{\frac{1}{2}}} \\ \frac{\tilde{y}+d_{sy}}{\left((\tilde{x}+\tilde{d}_{sx})^2+(\tilde{y}+\tilde{d}_{sy})^2+\tilde{z}^2\right)^{\frac{1}{2}}} \\ \frac{\tilde{z}}{\left((\tilde{x}+\tilde{d}_{sx})^2+(\tilde{y}+\tilde{d}_{sy})^2+\tilde{z}^2\right)^{\frac{1}{2}}} \end{bmatrix} \tag{23}$$

where $\tilde{d}_{mx}$, $\tilde{d}_{sx}$, and $\tilde{d}_{sy}$ of eqs. (23) are defined in eqs. (24-26). These quantities represent the positions of the Moon and Sun in the ephemeral coordinates. The transformed measurement model is given by eqs. (27-31).

$$\tilde{d}_{mx} = \mathbf{R}_{EM} \cdot \hat{\mathbf{e}}_{\tilde{x}} = \mathbf{R}_{EM} \cdot \frac{\mathbf{R}_{EM}}{||\mathbf{R}_{EM}||} = ||\mathbf{R}_{EM}|| \tag{24}$$

$$\tilde{d}_{sx} = \mathbf{R}_{ES} \cdot \frac{\mathbf{R}_{EM}}{||\mathbf{R}_{EM}||} \tag{25}$$

$$\tilde{d}_{sy} = \mathbf{R}_{ES} \cdot \left[\mathbf{R}_{ES} - \left(\mathbf{R}_{ES} \cdot \frac{\mathbf{R}_{EM}}{||\mathbf{R}_{EM}||}\right) \frac{\mathbf{R}_{EM}}{||\mathbf{R}_{EM}||}\right] \tag{26}$$

$$\zeta_1 = \cos\theta_{ecm} = \left[\frac{\tilde{x}^2 - \tilde{x}\tilde{d}_{mx} + \tilde{y}^2 + \tilde{z}^2}{(\tilde{x}^2+\tilde{y}^2+\tilde{z}^2)^{\frac{1}{2}} \left((\tilde{x}-\tilde{d}_{mx})^2 + \tilde{y}^2 + \tilde{z}^2\right)^{\frac{1}{2}}} \right] = h_1(\mathbf{x}) \tag{27}$$

$$\zeta_2 = \cos\theta_{ecs} = \left[\frac{\tilde{x}^2 - \tilde{x}\tilde{d}_{sx} + \tilde{y}^2 - \tilde{y}\tilde{d}_{sy} + \tilde{z}^2}{(\tilde{x}^2+\tilde{y}^2+\tilde{z}^2)^{\frac{1}{2}} \left((\tilde{x}-\tilde{d}_{sx})^2 + (\tilde{y}-\tilde{d}_{sy})^2 + \tilde{z}^2\right)^{\frac{1}{2}}} \right] = h_2(\mathbf{x}) \tag{28}$$

$$\zeta_3 = \cos\theta_{mcs} = \left[\frac{\tilde{x}^2 - \tilde{x}\tilde{d}_{mx} - \tilde{x}\tilde{d}_{sx} + \tilde{d}_{mx}\tilde{d}_{sx} + \tilde{y}^2 - \tilde{y}\tilde{d}_{sy} + \tilde{z}^2}{\left((\tilde{x}-\tilde{d}_{mx})^2 + \tilde{y}^2 + \tilde{z}^2\right)^{\frac{1}{2}} \left((\tilde{x}-\tilde{d}_{sx})^2 + (\tilde{y}-\tilde{d}_{sy})^2 + \tilde{z}^2\right)^{\frac{1}{2}}} \right] = h_3(\mathbf{x}) \tag{29}$$

$$\zeta_4 = \theta_e = 2\tan^{-1}\left(\frac{\tilde{d}_e}{\sqrt{\tilde{x}^2+\tilde{y}^2+\tilde{z}^2}} \right) = h_4(\mathbf{x}) \tag{30}$$

$$\zeta_5 = \theta_m = 2\tan^{-1}\left(\frac{\tilde{d}_m}{\sqrt{(\tilde{x}-\tilde{d}_{mx})^2+\tilde{y}^2+\tilde{z}^2}} \right) = h_5(\mathbf{x}) \tag{31}$$

In this transformed coordinate system, it becomes clear that the measurements cannot disambiguate the spacecraft position $(\tilde{x}, \tilde{y}, \tilde{z})$ from the position symmetrically across the plane $(\tilde{x}, \tilde{y}, -\tilde{z})$. This difficulty is apparent from the fact that the variable $\tilde{z}$ does not appear in any form other than its square, $\tilde{z}^2$. Thus, if the planets are in a non-singular configuration, the estimation process converges to whichever of the two optimal points is nearest to the initial guess. It is worth noting that one additional reference vector would eliminate this ambiguity. In the vicinity of the Galilean moons, for instance, position determination would be entirely unambiguous in non-singular configurations.

In the event that the Earth, Sun, and Moon align, ${}^eQ^E$ loses rank and the ephemeral frame becomes ill-defined. $\tilde{d}_{mx}$ and $\tilde{d}_{sx}$ of eqs. (24-25) remain defined, but $\tilde{d}_{sy}$ reduces to the zero vector. In this case, the measurement model reduces to the following:

$$\zeta_1 = \cos\theta_{ecm} = \left[\frac{\tilde{x}^2 - \tilde{x}\tilde{d}_{mx} + \left[\tilde{y}^2 + \tilde{z}^2\right]}{(\tilde{x}^2 + \left[\tilde{y}^2+\tilde{z}^2\right])^{\frac{1}{2}} \left((\tilde{x}-\tilde{d}_{mx})^2 + \left[\tilde{y}^2+\tilde{z}^2\right]\right)^{\frac{1}{2}}} \right] = h_1(\mathbf{x}) \tag{32}$$

$$\zeta_2 = \cos\theta_{ecs} = \left[\frac{\tilde{x}^2 - \tilde{x}\tilde{d}_{sx} + \left[\tilde{y}^2 + \tilde{z}^2\right]}{(\tilde{x}^2 + \left[\tilde{y}^2+\tilde{z}^2\right])^{\frac{1}{2}} \left((\tilde{x}-\tilde{d}_{sx})^2 + \left[\tilde{y}^2+\tilde{z}^2\right]\right)^{\frac{1}{2}}} \right] = h_2(\mathbf{x}) \tag{33}$$

$$\zeta_3 = \cos\theta_{mcs} = \left[\frac{\tilde{x}^2 - \tilde{x}\tilde{d}_{mx} - \tilde{x}\tilde{d}_{sx} + \tilde{d}_{mx}\tilde{d}_{sx} + \left[\tilde{y}^2 + \tilde{z}^2\right]}{\left((\tilde{x}-\tilde{d}_{mx})^2 + \left[\tilde{y}^2+\tilde{z}^2\right]\right)^{\frac{1}{2}} \left((\tilde{x}-\tilde{d}_{sx})^2 + \left[\tilde{y}^2+\tilde{z}^2\right]\right)^{\frac{1}{2}}} \right] = h_3(\mathbf{x}) \tag{34}$$

$$\zeta_4 = \theta_e = 2\tan^{-1}\left(\frac{\tilde{d}_e}{\sqrt{\tilde{x}^2+\left[\tilde{y}^2+\tilde{z}^2\right]}} \right) = h_4(\mathbf{x}) \tag{35}$$

$$\zeta_5 = \theta_m = 2\tan^{-1}\left(\frac{\tilde{d}_m}{\sqrt{(\tilde{x}-\tilde{d}_{mx})^2+\left[\tilde{y}^2+\tilde{z}^2\right]}} \right) = h_5(\mathbf{x}) \tag{36}$$

While $\tilde{x}$ remains defined, $\tilde{y}$ and $\tilde{z}$ now only appear in the measurement equations as the coupled quantity $\left[\tilde{y}^2 + \tilde{z}^2\right]$. In this case, the measurement model is no longer able to discern between any two points that are equidistant from the vector from the Earth to the Moon. The Gauss-Newton iteration converges to whichever point on this ring is nearest to the initial guess. This can lead to inaccurate answers, though the Gauss-Newton method can also accurately calculate the error in these estimates. As the celestial bodies approach alignment, $\tilde{d}_{sy}$ approaches zero. Thus, the problem can become ill-conditioned without becoming fully singular.

Another question to answer is how significantly, if at all, the position estimate would improve if the attitude determination problem were solved first. In this case, one would be able to measure the angle of separation between two celestial bodies in the range $[0, 2\pi]$ rather than simply the magnitude of separation in the range $[0, \pi]$. One way of representing all of this information is to add the sine of the angles of separation to the measurement model. Doing so reduces the number of possible angular separations from two to one, fully specifying the system. The sine is obtained by taking the square root (ambiguously signed) of one minus the square of the cosine of the angle.

$$\zeta_1 = \cos\theta_{ecm} = \left[\frac{\tilde{x}^2 - \tilde{x}\tilde{d}_{mx} + \tilde{y}^2 + \tilde{z}^2}{(\tilde{x}^2 + \tilde{y}^2 + \tilde{z}^2)^{\frac{1}{2}} \left((\tilde{x} - \tilde{d}_{mx})^2 + \tilde{y}^2 + \tilde{z}^2 \right)^{\frac{1}{2}}} \right] = h_1(\mathbf{x}) \tag{37}$$

$$\zeta_2 = \cos\theta_{ecs} = \left[\frac{\tilde{x}^2 - \tilde{x}\tilde{d}_{sx} + \tilde{y}^2 - \tilde{y}\tilde{d}_{sy} + \tilde{z}^2}{(\tilde{x}^2 + \tilde{y}^2 + \tilde{z}^2)^{\frac{1}{2}} \left((\tilde{x} - \tilde{d}_{sx})^2 + (\tilde{y} - \tilde{d}_{sy})^2 + \tilde{z}^2 \right)^{\frac{1}{2}}} \right] = h_2(\mathbf{x}) \tag{38}$$

$$\zeta_3 = \cos\theta_{mcs} = \left[\frac{\tilde{x}^2 - \tilde{x}\tilde{d}_{mx} - \tilde{x}\tilde{d}_{sx} + \tilde{d}_{mx}\tilde{d}_{sx} + \tilde{y}^2 - \tilde{y}\tilde{d}_{sy} + \tilde{z}^2}{\left((\tilde{x} - \tilde{d}_{mx})^2 + \tilde{y}^2 + \tilde{z}^2 \right)^{\frac{1}{2}} \left((\tilde{x} - \tilde{d}_{sx})^2 + (\tilde{y} - \tilde{d}_{sy})^2 + \tilde{z}^2 \right)^{\frac{1}{2}}} \right] = h_3(\mathbf{x}) \tag{39}$$

$$\zeta_4 = \theta_e = 2\tan^{-1}\left(\frac{\tilde{d}_e}{\sqrt{\tilde{x}^2 + \tilde{y}^2 + \tilde{z}^2}} \right) = h_4(\mathbf{x}) \tag{40}$$

$$\zeta_5 = \theta_m = 2\tan^{-1}\left(\frac{\tilde{d}_m}{\sqrt{(\tilde{x} - \tilde{d}_{mx})^2 + \tilde{y}^2 + \tilde{z}^2}} \right) = h_5(\mathbf{x}) \tag{41}$$

$$\zeta_6 = \sin\theta_{ecm} = \pm\sqrt{1 - \left[\frac{\tilde{x}^2 - \tilde{x}\tilde{d}_{mx} + \tilde{y}^2 + \tilde{z}^2}{(\tilde{x}^2 + \tilde{y}^2 + \tilde{z}^2)^{\frac{1}{2}} \left((\tilde{x} - \tilde{d}_{mx})^2 + \tilde{y}^2 + \tilde{z}^2 \right)^{\frac{1}{2}}} \right]^2} = h_6(\mathbf{x}) \tag{42}$$

$$\zeta_7 = \sin\theta_{ecs} = \pm\sqrt{1 - \left[\frac{\tilde{x}^2 - \tilde{x}\tilde{d}_{sx} + \tilde{y}^2 - \tilde{y}\tilde{d}_{sy} + \tilde{z}^2}{(\tilde{x}^2 + \tilde{y}^2 + \tilde{z}^2)^{\frac{1}{2}} \left((\tilde{x} - \tilde{d}_{sx})^2 + (\tilde{y} - \tilde{d}_{sy})^2 + \tilde{z}^2 \right)^{\frac{1}{2}}} \right]^2} = h_7(\mathbf{x}) \tag{43}$$

$$\zeta_8 = \sin\theta_{mcs} = \pm\sqrt{1 - \left[\frac{\tilde{x}^2 - \tilde{x}\tilde{d}_{mx} - \tilde{x}\tilde{d}_{sx} + \tilde{d}_{mx}\tilde{d}_{sx} + \tilde{y}^2 - \tilde{y}\tilde{d}_{sy} + \tilde{z}^2}{\left((\tilde{x} - \tilde{d}_{mx})^2 + \tilde{y}^2 + \tilde{z}^2 \right)^{\frac{1}{2}} \left((\tilde{x} - \tilde{d}_{sx})^2 + (\tilde{y} - \tilde{d}_{sy})^2 + \tilde{z}^2 \right)^{\frac{1}{2}}} \right]^2} = h_8(\mathbf{x}) \tag{44}$$

The quantity in the square root of eqs. (42-44) can be obtained without solving the attitude problem. The only information that is unavailable is the sign on the square root. Solving the attitude problem introduces this information to the system, but no more. In other words, the attitude information introduces binary information to the system: positive or negative on each square root.

This binary information cannot introduce additional information about the magnitude of any of the position coordinates; it can introduce only information about the sign of the coordinates. This is the most information that can be carried by the sign of these measurements. The signs of the $\tilde{x}$ and $\tilde{y}$ position coordinates are already known unambiguously given just the cosine information; so, the attitude information introduces information about the sign of the $\tilde{z}$ coordinate in the ephemeral coordinates. That is to say, it reduces the number of possible locations from two to one, but it does not introduce any additional accuracy in that correct position. By decoupling the attitude and position problems, one accepts the inherent ambiguities described in this section. One does not, however, sacrifice the accuracy with which any one of these positions is known. Therefore, estimating the position without attitude determination is not a design trade-off at the system level. The choice of attitude sensors can be made regardless of the requirements on accuracy of the navigation estimate.

IV.C. Noise Model

Each of these measurements has noise associated with it, which must be modeled by the measurement error covariance matrix R. The error in each cosine measurement stems from error in unit-vector measurements to the center of each celestial body. The errors in unit-vector measurements stem from error in centroid determination, which in turn involves the precision and accuracy of the camera (including its optics), and the image-processing algorithms. One can therefore solve for the error covariance matrix for the cosine measurements by propagating error in centroid determination.

$$E_{centroid} = \mathcal{N}(0, \delta^2) \text{ (measured in pixels)} = \mathcal{N}(0, s_p^2\delta^2) \text{ (measured in meters)} \tag{45}$$

Eq. (45) transforms error in pixel measurement to units of meters by scaling the error by the size of each pixel, s_p. δ^2 is the variance of the error in pixel measurements. For this analysis, it is assumed that the standard deviation of the error in pixel measurements is $\frac{1}{10}$ of a pixel, and that the pixel size is 1.4×10^{-6} meters. Assuming a known camera field of view (Θ) and pixel resolution (P), the above pixel error can be transformed into angular measurement error via eq. (46). For this analysis, a pixel resolution of $P = 2500 \times 2500$ pixels and a field of view of $\Theta = 0.872$ radians is assumed.

$$E_{angular} = \frac{\Theta}{P}\mathcal{N}\left(0, \delta^2\right) = \mathcal{N}\left(0, \frac{\delta^2\Theta^2}{P^2}\right) \tag{46}$$

Eq. (46) assumes independence of all angular measurements (an approximately true assumption, though not exactly true). The measurement error of the angle between two independent unit vectors, therefore, is given by $\mathcal{N}\left(0, \frac{2\delta^2\Theta^2}{P^2}\right)$. This information can be used to determine error in the cosine measurements (also assumed independent, though there exist some small cross terms). Letting θ_m be the measured angular separation, and $\delta\theta$ be a small deviation from that angle, eqs. (47-48) show how small angle errors influence cosine measurements.

$$\cos\left(\theta_m + \delta\theta\right) = \cos\theta_m \cos\delta\theta + \sin\theta_m \sin\delta\theta \tag{47}$$

$$\approx \cos\theta_m + \delta\theta \sin\theta_m \tag{48}$$

The sine of the angle is not directly observable. Instead, it is ascertained from the cosine measurement. Eqs. (49-51) show how the sine term is generated from the cosine measurement.

$$\cos\left(\theta_m + \delta\theta\right) \approx \cos\theta_m + \delta\theta\left[\pm\sqrt{1 - \cos^2\theta_m}\right] \tag{49}$$

$$\approx \cos\theta_m + \mathcal{N}\left(0, \frac{2\delta^2\Theta^2}{P^2}\right)\left[\pm\sqrt{1 - \cos^2\theta_m}\right] \tag{50}$$

$$\approx \cos\theta_m + \mathcal{N}\left(0, \left[1 - \cos^2\theta_m\right]\frac{2\delta^2\Theta^2}{P^2}\right) \tag{51}$$

Because the cosine is constrained to [-1,1], the noise term decreases to zero at these limits in order to prevent illegal cosines. If the quantity being measured were an angle rather than the magnitude or cosine of an angle, then the error would not depend on the relative positions of the two planets being measured. No matter the relative positions of the planets, the expected angle measurement would be the same. This principle does not hold for magnitude/cosine measurements where the rate of change of measurements with small deviations in angular separation depends on the angular separation itself. Thus, the error covariance for the cosine measurements is a function of the measurements themselves. With eq. (46) and eq. (51), it is possible to construct the full measurement-error covariance matrix $R(\zeta)$.

$$R(\zeta) \approx \begin{bmatrix} \frac{2\delta^2\Theta^2}{P^2}\left[1 - \zeta_1^2\right] & 0 & 0 & 0 & 0 \\ 0 & \frac{2\delta^2\Theta^2}{P^2}\left[1 - \zeta_2^2\right] & 0 & 0 & 0 \\ 0 & 0 & \frac{2\delta^2\Theta^2}{P^2}\left[1 - \zeta_3^2\right] & 0 & 0 \\ 0 & 0 & 0 & \frac{\delta^2\Theta^2}{P^2} & 0 \\ 0 & 0 & 0 & 0 & \frac{\delta^2\Theta^2}{P^2} \end{bmatrix} \tag{52}$$

The approximately equals symbol in eq. (52) reflects that some small cross terms are being omitted from the measurement error covariance matrix. These measurements, and their 3σ errors, can be visualized over the course of the entire true trajectory. See Figures 4 and 5.

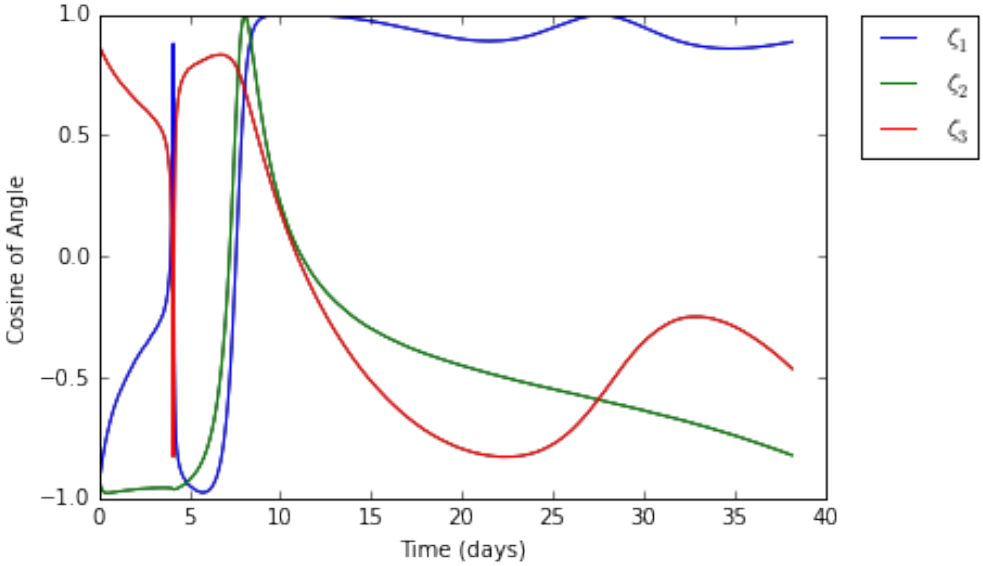

Figure 4: Cosine of angular separation measurmements throughout trajectory

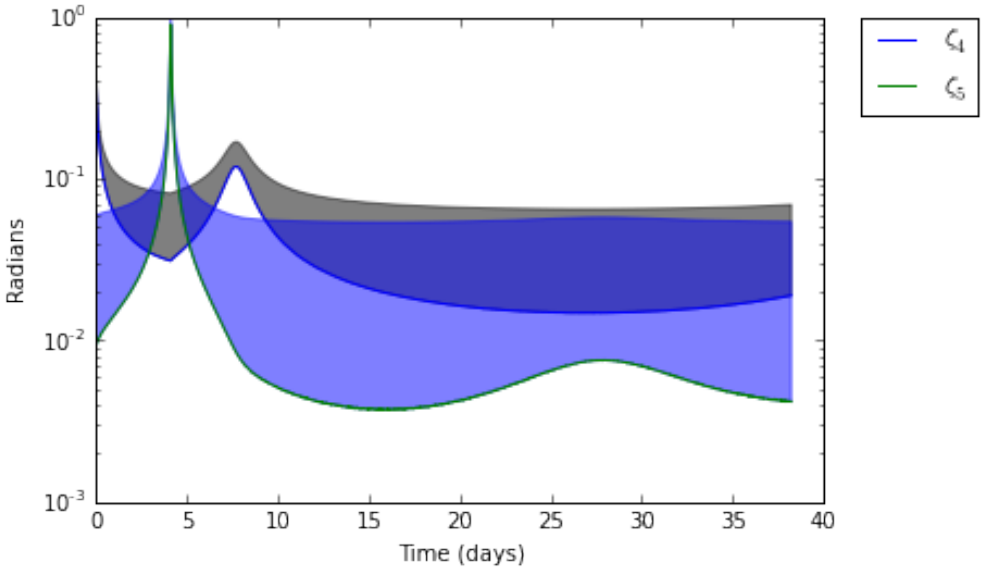

Figure 5: Earth and Moon angular width measurements throughout trajectory

IV.D. Gauss-Newton Iteration

Given a set of measurements ζ, the optimal estimate for the state $\mathbf{x}$ is that which minimizes the weighted nonlinear cost function of eq. (53). By transforming ζ and h with the inverse transpose of the Cholesky factorization of the measurement error covariance, this function can be transformed to an unweighted nonlinear cost. Since the measurement-error covariance is a diagonal matrix, this transformation is easy to obtain. Eqs. (54-55) create a transformation matrix from the inverse transpose of the Cholesky factorization of the measurement error covariance, and eq. (56) transforms the nonlinear weighted cost function to an unweighted cost function.

$$J(\mathbf{x}) = \frac{1}{2}\left[\zeta - h(\mathbf{x})\right]^T R^{-1}\left[\zeta - h(\mathbf{x})\right] \tag{53}$$

$$R = R_a^T R_a \longrightarrow R_a = \begin{bmatrix} \sqrt{\frac{2\delta^2\Theta^2}{P^2}\left[1-\zeta_1^2\right]} & 0 & 0 & 0 & 0 \\ 0 & \sqrt{\frac{2\delta^2\Theta^2}{P^2}\left[1-\zeta_2^2\right]} & 0 & 0 & 0 \\ 0 & 0 & \sqrt{\frac{2\delta^2\Theta^2}{P^2}\left[1-\zeta_3^2\right]} & 0 & 0 \\ 0 & 0 & 0 & \sqrt{\frac{\delta^2\Theta^2}{P^2}} & 0 \\ 0 & 0 & 0 & 0 & \sqrt{\frac{\delta^2\Theta^2}{P^2}} \end{bmatrix} \tag{54}$$

$$\longrightarrow R_a^{-T} = \begin{bmatrix} \frac{1}{\sqrt{\frac{2\delta^2\Theta^2}{P^2}\left[1-\zeta_1^2\right]}} & 0 & 0 & 0 & 0 \\ 0 & \frac{1}{\sqrt{\frac{2\delta^2\Theta^2}{P^2}\left[1-\zeta_2^2\right]}} & 0 & 0 & 0 \\ 0 & 0 & \frac{1}{\sqrt{\frac{2\delta^2\Theta^2}{P^2}\left[1-\zeta_3^2\right]}} & 0 & 0 \\ 0 & 0 & 0 & \sqrt{\frac{P^2}{\delta^2\Theta^2}} & 0 \\ 0 & 0 & 0 & 0 & \sqrt{\frac{P^2}{\delta^2\Theta^2}} \end{bmatrix} \tag{55}$$

$$\zeta_a = R_a^{-T}\zeta \qquad h_a = R_a^{-T}h(\mathbf{x}) \qquad w_a = R_a^{-T}w \tag{56}$$

The nonlinear unweighted cost function is shown in eq. (57). The goal now is to find the $\mathbf{x}$ that minimizes this function using Gauss-Newton iteration. Dropping the a subscript for convenience, the first-order necessary condition for $J(\mathbf{x})$ optimality is given by eq. (58).

$$J_a(\mathbf{x}) = \frac{1}{2}\left[\zeta_a - h_a(\mathbf{x})\right]^T\left[\zeta_a - h_a(\mathbf{x})\right] \tag{57}$$

$$\mathbf{0} = \left[\frac{\partial J}{\partial \mathbf{x}}\right]^T = \left[\zeta - h(\mathbf{x})\right]^T\left[-\frac{\partial h}{\partial \mathbf{x}}\right] = -\left[\zeta - h(\mathbf{x})\right]^T H \tag{58}$$

With no prior knowledge, there would be a huge search space to traverse in order to find the absolute minimum that satisfies the first-order optimality condition of eq. (58). However, an initial guess can be generated using the nominal trajectory, and a hill-climber algorithm can then be used to reach the local extremum in the vicinity of the initial guess. Beginning with an initial guess $\mathbf{x}_g$, eqs. (59-60) solve for the deviation in position, $\mathbf{\Delta x}$ that moves towards the optimal solution.

$$0 = f(\mathbf{x}_g + \Delta\mathbf{x}_g) \approx f(\mathbf{x}_g) + \left[\frac{\partial f}{\partial \mathbf{x}}\right]_{\mathbf{x}_g}\Delta\mathbf{x} \tag{59}$$

$$\Delta\mathbf{x} = -\left[\frac{\partial f}{\partial \mathbf{x}}\right]^{-1} f(\mathbf{x}_g) \tag{60}$$

With the corrective step $\mathbf{\Delta x}$, a new guess is formed $\mathbf{x}_{g,new} = \mathbf{x}_g + \Delta\mathbf{x}$ and the process is repeated until convergence. This local optimization method requires the derivative of the nonlinear cost function with respect to the state vector $\mathbf{x}$. This derivative is shown in eq. (61).

$$\frac{\partial f}{\partial \mathbf{x}} = -\frac{\partial (H^T)}{\partial \mathbf{x}}\left[\zeta - h(\mathbf{x})\right] + H^T(\mathbf{x})\frac{\partial h}{\partial \mathbf{x}} = V \tag{61}$$

Eq. (61) can be simplified under the assumption that the initial guess (provided either by the nominal trajectory or a dynamics model) places the spacecraft in the vicinity of the optimal solution. Under these conditions, $z - h(\mathbf{x}) \approx 0$ and eq. (61) reduces to eq. (62).

$$\frac{\partial f}{\partial \mathbf{x}} \approx H^T H = V \tag{62}$$

Under these conditions, eq. (60) may be rewritten as eqs. (63-64). In eqs. (63-64), $\tilde{R}$ and $\tilde{Q}$ are the R and Q of the QR factorization of H_a, the Jacobian of the nonlinear measurement equations $h(\mathbf{x})$ with respect to $\mathbf{x}$, transformed by the inverse transpose of the Cholesky factorization of the measurement error covariance.

$$\Delta\mathbf{x} = V^{-1}\left\{H^T\left[\zeta - h(\mathbf{x}_g)\right]\right\} \tag{63}$$

$$= \tilde{R}^{-1}\tilde{Q}^T\left[\zeta - h(\mathbf{x})\right] \tag{64}$$

A line search can be implemented to converge as quickly as possible to the optimal solution. With each iteration, let $\mathbf{x}_{g,new} = \mathbf{x}_g + \alpha\Delta\mathbf{x}$ with $0 < \alpha \leq 1$ chosen to enforce $J(\mathbf{x}_g + \alpha\Delta\mathbf{x}) < J(\mathbf{x}_g)$. The following method can be used to enforce this:

1. Set α=1
2. Set $J_g = J(\mathbf{x}_g)$
3. Set $J_{g,new} = J(\mathbf{x}_g + \alpha\Delta\mathbf{x})$
4. While $J_{g,New} \geq J_g$:
   $\alpha = \frac{\alpha}{2}$
   $J_{gNew} = J(\mathbf{x}_g + \alpha\Delta\mathbf{x})$

The line search is terminated when α is halved 100 times. The error covariance for each position estimate is estimated by taking $P = \left(H^T H\right)^{-1}$.

IV.E. Gauss-Newton Extended Kalman Filter

With a dynamics model, one can construct an Extended Kalman filter with the Gauss-Newton position and error covariance estimates as the measurement and measurement covariance inputs to the filter. Doing so propagates the spacecraft through the singular configurations described in section IV.B, at the cost of implementation complexity. The resulting filter is unique in that the measurements, ζ, depend on the state propagation estimates $\mathbf{x}(k+1|k)$. In other words, the initial guess for the Gauss-Newton iteration (the measurement model for the EKF) is provided by the dynamic propagation for the EKF. For the trajectory being treated here, the dynamics model is simply the orbital propagation of the spacecraft under the influence of Earth, Sun, and Moon gravity with process noise covariance given by eq. (4).

V. Results

At each timestep, separated by 30 minutes, the Gauss-Newton method uses ephemerides information to establish the geometry of the Earth, Sun, Moon system. For non-singular configurations (configurations in which the Earth, Sun, and Moon span R^2), the iteration converges to one of two possible locations given an initial guess that can be many thousands of kilometers from the true location. Figure 6 shows the cost and stepsize decreasing for a set of measurements taken at time $t = 0$. The Gauss-Newton method was initialized with a guess 170,000 km from the true position, and converged to a position 7 km from the true position.

Figures 7 and 8 show the position determination error throughout the entire trajectory, with the 3σ estimated error also overlayed in Figure 8. At each timestep, the spacecraft attitude is randomized and the Gauss-Newton iteration is initialized with the position given by the nominal trajectory. As shown in Figure 3, these initial guesses may be up to 10,000 kilometers from the true spacecraft location. The Gauss-Newton confidently converges to within tens of kilometers in nonsingular configurations, and the error spikes in singular configurations. These spokes reflect the fact that the celestial bodies nearly align at these times, and the number of possible positions from one set of measurements increases from two to an infinite number lying on a ring surrounding the vector to all celestial bodies. Figures 9 and 10 inclusion of a dynamics model in the Gauss-Newton Extended Kalman Filter can smooth over these spikes.

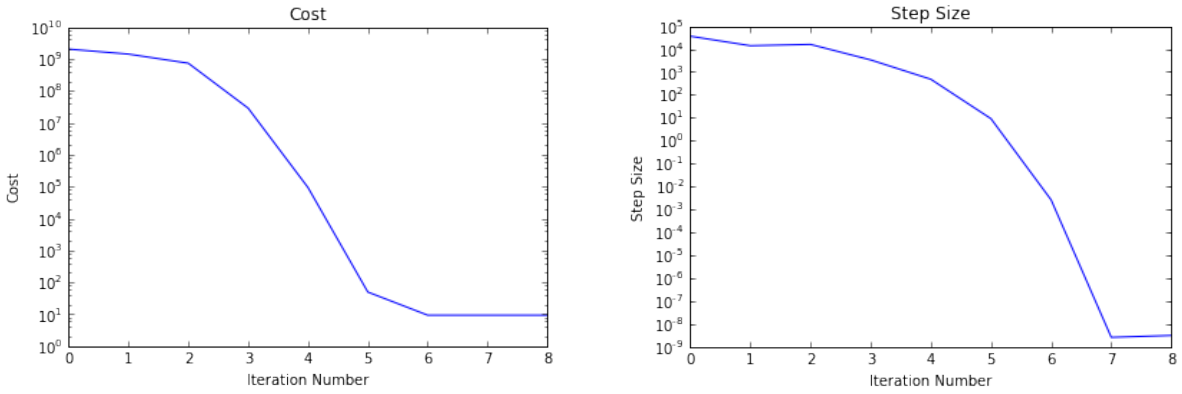

(a) Cost decreasing

(b) Stepsize decreasing

Figure 6: Convergence of Gauss-Newton iteration at $t = 0$, initial guess 170,000 km from true position, convergence to 7 km from true position

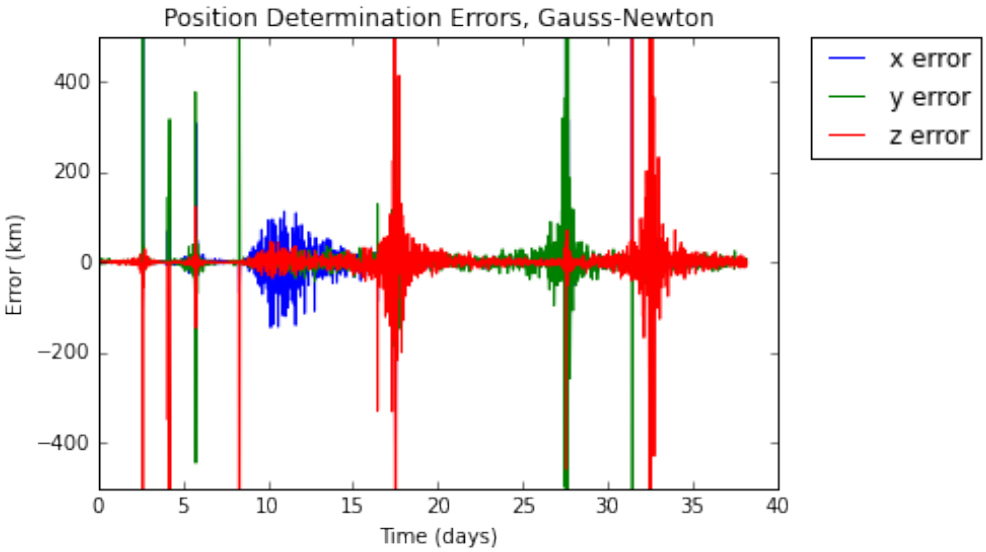

Figure 7: Position determination error throughout entire trajectory, initial guesses from nominal trajectory

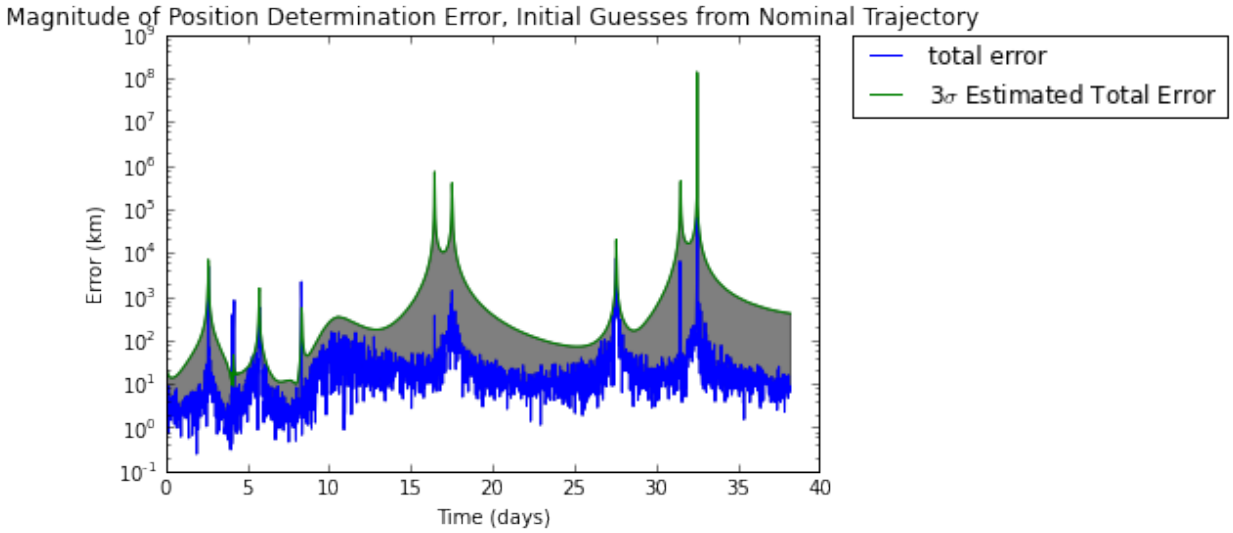

Figure 8: Magnitude of position determination error throughout entire trajectory, initial guesses from nominal trajectory

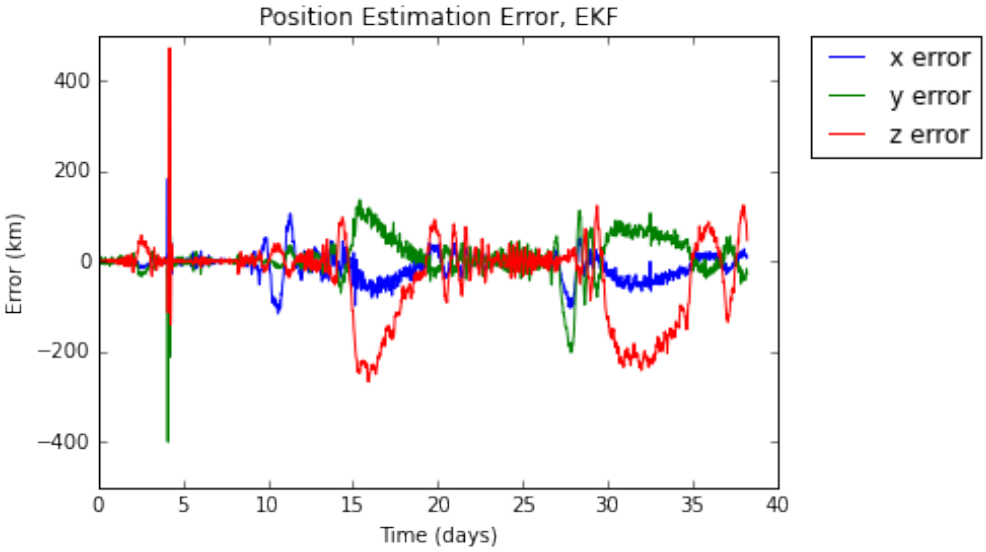

Figure 9: Position estimation error for Gauss-Newton Extended Kalman Filter

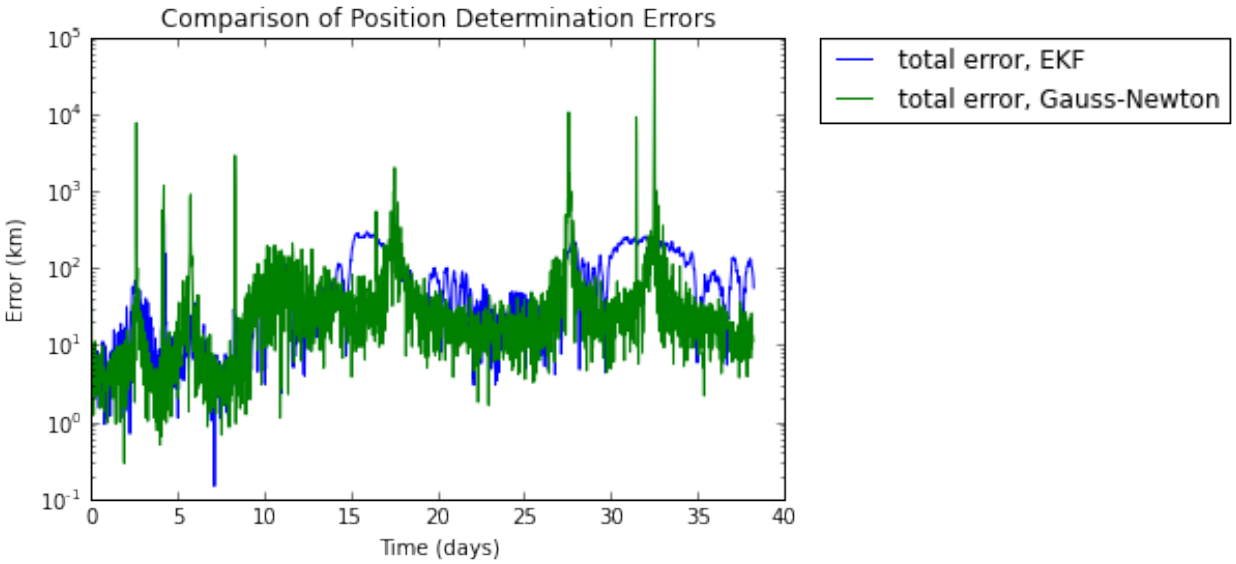

Figure 10: Error comparison for Gauss-Newton estimates and Extended Kalman Filter estimates

VI. Conclusion

The analysis shows that this optical navigation technique is a promising approach for low-cost, low-power navigation in regions of space occupied by planets, moons, and the sun, and any other objects that are significantly brighter than background stars. The simulated trans-lunar trajectory verifies the correctness of the analysis and shows that the technique is capable of determining position to within tens of kilometers in non-singular configurations of the celestial bodies. This analysis has assumed the camera parameters of a Raspberry Pi camera module, which is readily adapted to CubeSat use. It has assumed that the error in measurement of centroid and width of celestial bodies is Gaussian with a standard deviation of $\frac{1}{10}$ of a pixel. The inclusion of a dynamics model by means of a Gauss-Newton Extended Kalman Filter smooths over the singular regions where the measurement model is unable to discern multiple points in space. By eliminating the need for simultaneous attitude estimation, the filter and related computations are much simpler than one might expect. Running the EKF may not be necessary, depending on the accuracy required, since the Gauss-Newton solver provides comparable performance.

The method is sensitive to the initial guess with which it is provided in that it converges to the nearest point in space that agrees with the measurements. In non-singular configurations, this is one of two locations. In singular configurations, this is one of infinite locations lying on a ring surrounding the line containing the three reference bodies. In a more densely populated region of space, these singularities would become less frequent and the ambiguities would generally disappear.

The navigation method described in this paper assumes access to time. A future analysis will explore the lost-in-space scenario in which the spacecraft has no knowledge of position, attitude, or time and must deduce its location from optical measurements. Future work includes the verification of these simulated results on a hardware testbed, with the objective of a flight demonstration in early 2018.

References

[1]Cherubini, Andrea, Fabien Spindler, and Francois Chaumette. "Autonomous Visual Navigation and Laser-Based Moving Obstacle Avoidance." IEEE Trans. Intell. Transport. Syst. IEEE Transactions on Intelligent Transportation Systems: 2101-110. Print.

[2]Christian, John (2010). Optical Navigation for a Spacecraft in a Planetary System. Retrieved from UT Austin Repositories.

[3]Christian, John, and E. Glenn Lightsey. "Integrated Performance of an Autonomous Optical Navigation System for Space Exploration." AIAA SPACE 2010 Conference & Exposition (2010). Print.

[4]Lightsey, Glenn E., and John A. Christian. "Onboard Image-Processing Algorithm for a Spacecraft Optical Navigation Sensor System." Journal of Spacecraft and Rockets: 337-52. Print.

[5]Lu, Feng, and Evangelos Milios. "Robot pose estimation in unknown environments by matching 2d range scans." Journal of Intelligent and Robotic Systems 18.3 (1997): 249-275.

[6]Markley, F. L. (Director) (1999, August 16). How to Estimate Attitude from Vector Observations. AAS/AIAA Astrodynamics Specialist Conference. Lecture conducted from AIAA, .

[7]Marshall, William, and Chris Boshuizen. "Planet Labs' Remote Sensing Satellite System." (2013).

[8]Shin, Dong, Durgadas Bagri, and James Border. "Advanced Calibration Technique for Accurate Three-Way Spacecraft Ranging." Interplanetary Network Progress Report 199 (2014): 1.

[9]"Small Spacecraft Technology State of the Art," NASA/TP 2014 216648/rev1, Ames Research Center, Moffett Field, CA.

[10]Swartwout, Michael. "The first one hundred CubeSats: A statistical look." JoSS 2pp (2014): 213-233.

[11]Zhang, Zhengyou. "A flexible new technique for camera calibration." Pattern Analysis and Machine Intelligence, IEEE Transactions on 22.11 (2000): 1330-1334.